Alkanethiol-Induced Structural Rearrangements in Silica−Gold Core−Shell-type Nanoparticle Clusters: An Opportunity for Chemical Sensor Engineering

Frank Osterloh,* Hiroki Hiramatsu, Rhiannon Porter, and Ting Guo*

Department of Chemistry, University of California, One Shields Avenue, Davis, California 95616

Received May 21, 2003. In Final Form: April 19, 2004

Electrostatically bonded SiO_2·Au nanoparticle clusters form by reaction of 3-aminopropylsilane-modified SiO_2 spheres (470 nm) with citrate-coated gold nanoparticles (9.7 nm) in water. Reaction of the clusters with 0.01 M KBr or HCl solution induces desorption of the gold nanoparticles within minutes. Reaction of the clusters with alkanethiols $C_nH_{2n+1}SH$ ($n = 2-18$) at 80 °C causes the gold nanoparticles to form stringlike gold nanoparticle structures for thiols with short alkane groups ($n = 2, 3, 4$) and hexagonally packed arrays of gold nanoparticles for thiols with long alkane groups ($n = 5-18$) on the silica surfaces. The structural changes indicate that the bonding between Au and SiO_2 nanoparticles has changed from electrostatic to van der Waals. Elemental analyses show that the reaction with hexanethiol does not affect the Au/Si/O composition of the SiO_2·Au composite, and Raman spectra on the hexanethiol-reacted material indicate the formation of a thiol SAM on the gold nanoparticles. The thiol-reacted SiO_2·Au clusters display characteristic shifts of the absorption maxima in the visible spectra, and there is an inverse relation between these shifts and the lengths of the alkyl groups in the thiols. This relationship can be understood in terms of the free electron model for metals. The use of SiO_2·Au nanoparticle clusters as coulometric sensors for the qualitative detection of thiols is discussed.

Introduction

As nanoparticle-based bottom-up assembly strategies to materials and devices continue to evolve,[1−7] it become increasingly important to understand and control the bonding interactions between inorganic nanoparticles. The nature of the nanoparticle−nanoparticle bond profoundly influences the collective chemical and physical properties of the material. The bonding determines the stability of the aggregate and its reactivity with small molecules and other nanoparticles,[8] and the distance between the bonded nanoparticles affects the electronic and magnetic coupling between inorganic components.

Core−shell-type SiO_2·Au clusters of the general structure shown in Figure 1 provide a convenient medium to study the influence of the bonding on the properties of a nanoparticle aggregate. These clusters consist of Au nanoparticles that are attached to the surfaces of submicrometer SiO_2 spheres by means of organic linkers. Groups with various linkage capabilities can be readily introduced to the surface of the silica particles by means of organosilanes[9−11] and to the gold nanoparticles by means of thiols.[12−15] Appropriate modifications and reactions of the functionalized nanoparticles have allowed the synthesis of a variety of electrostatically and covalently bonded SiO_2·Au clusters (see Figure 1 and Table 1),[8,16−19] some of which have been proposed for electromagnetic signal processing applications[20−22] and as biosensors.[19]

We report here on the electrostatic assembly of 3-aminopropylsilane-terminated 470-nm silica spheres and citrate-coated gold (9.7 nm) nanoparticles and on the reactions of the resultant SiO_2·Au core−shell-type aggregates with electrolytes and with various linear chain alkanethiols. As we will show, alkanethiols can cause structural rearrangements of the SiO_2·Au clusters, which are accompanied with characteristic changes of their optical spectra. The stereochemical nonrigidity of the formed van der Waals bonded clusters is interesting for the design of nanoparticle-based switches, which can exist in two different states with different physical properties. Potential uses of SiO_2·Au nanoparticle clusters as sensor elements for the detection of alkanethiols will be discussed.

* To whom correspondence should be addressed. Phone: 530 754 6242. Fax: 530 752 8992. E-mail: osterloh@chem.ucdavis.edu.

(1) Lieber, C. M. *Sci. Am.* **2001**, *285*, 58−64.
(2) Fendler, J. H. *Chem. Mater.* **1996**, *8*, 1616−1624.
(3) Gracias, D. H.; Tien, J.; Breen, T. L.; Hsu, C.; Whitesides, E. M. *Science* **2000**, *289*, 1170−1172.
(4) Yin, Y. D.; Lu, Y.; Xia, Y. N. *J. Mater. Chem.* **2001**, *11*, 987−989.
(5) Porter, L. A.; Choi, H. C.; Schmeltzer, J. M.; Ribbe, A. E.; Elliott, L. C. C.; Buriak, J. M. *Nano Lett.* **2002**, *2*, 1369−1372.
(6) Giraldo, O.; Marquez, M.; Brock, S. L.; Suib, S. L.; Hillhouse, H.; Tsapatsis, M. *J. Am. Chem. Soc.* **2000**, *122*, 12158−12163.
(7) Cumberland, S. L.; Berrettini, M. G.; Javier, A.; Strouse, G. F. *Chem. Mater.* **2003**, *15*, 1047−1056.
(8) Hiramatsu, H.; Osterloh, F. E. *Langmuir* **2003**, *19*, 7003−7011.
(9) Ulman, A. *Chem. Rev.* **1996**, *96*, 1533−1554.
(10) Boerio, F. J.; Armogan, L.; Cheng, S. Y. **1980**, *73*, 416.
(11) Grabar, K. C.; Allison, K. J.; Baker, B. E.; Bright, R. M.; Brown, K. R.; Freeman, R. G.; Fox, A. P.; Keating, C. D.; Musick, M. D.; Natan, M. J. *Langmuir* **1996**, *12*, 2353−2361.
(12) Weisbecker, C. S.; Merritt, M. V.; Whitesides, G. M. *Langmuir* **1996**, *12*, 3763−3772.
(13) Hasan, M.; Bethell, D.; Brust, M. *J. Am. Chem. Soc.* **2002**, *124*, 1132−1133.
(14) Liu, G. Y.; Xu, S.; Qian, Y. L. *Acc. Chem. Res.* **2000**, *33*, 457−466.
(15) Tamada, K.; Ishida, T.; Knoll, W.; Fukushima, H.; Colorado, R.; Graupe, M.; Shmakova, O. E.; Lee, T. R. *Langmuir* **2001**, *17*, 1913−1921.
(16) Westcott, S. L.; Oldenburg, S. J.; Lee, T. R.; Halas, N. J. *Langmuir* **1998**, *14*, 5396−5401.
(17) Sadtler, B.; Wei, A. *Chem. Commun.* **2002**, 1604−1605.
(18) Galow, T. H.; Boal, A. K.; Rotello, V. M. *Adv. Mater.* **2000**, *12*, 576−579.
(19) Fleming, M. S.; Walt, D. R. *Langmuir* **2001**, *17*, 4836−4843.
(20) Westcott, S. L.; Oldenburg, S. J.; Lee, T. R.; Halas, N. J. *Chem. Phys. Lett.* **1999**, *300*, 651−655.
(21) Oldenburg, S. J.; Averitt, R. D.; Westcott, S. L.; Halas, N. J. *Chem. Phys. Lett.* **1998**, *288*, 243−247.
(22) Oldenburg, S. J.; Hale, G. D.; Jackson, J. B.; Halas, N. J. *Appl. Phys. Lett.* **1999**, *75*, 1063−1065.

10.1021/la0348719 CCC: $27.50
Published on Web 00/00/0000 PAGE EST: 5.2

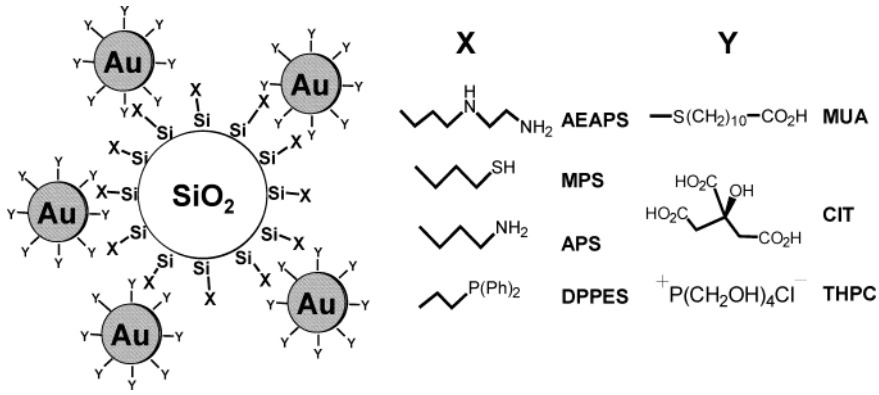

Figure 1. Schematic composition of electrostatically and covalently bonded silica−gold core−shell-type nanoparticle composites.

Table 1. Ligand and Bonding Types Employed in SiO_2·Au Core−Shell-type Nanoparticle Clusters

X^a	Y^a	bonding	reference
APS	MUA	electrostatic	8, 18
APS	THPC	covalent	16
MPS	THPC	covalent	16
DPPES	THPC		16
MPS	CIT	covalent	19
APS		covalent	20−22
APS	$C_nH_{(2n+1)}SH$ ($n = 2-18$)	van der Waals	this paper
APS	CIT	electrostatic	this paper
AEAPS	CIT	electrostatic	17

[a] For abbreviations, see Figure 1.

Experimental Section

The 470 ± 40 nm diameter silica spheres were synthesized by hydrolysis of 2.92 g of tetraethoxysilane in a 5 M NH_3 solution of 50 mL ethanol and 1.8 g of water according to the procedure of Stoeber et al.[25] The particles were subsequently functionalized with 3-aminopropyltrimethoxysilane as described previously[8] and converted into the hydrochloride by addition of concentrated hydrochloric acid. A solution of citrate-stabilized gold particles (9.7 ± 1.0 nm) was synthesized according to the procedure by Frens,[26] by adding 600 mg of sodium citrate in 60 mL of water to a boiling solution of 180 mg of tetrachloroaurate in 590 mL of water. After 2 h of reflux, the gold colloid solution was cooled to room temperature and stored at 5 °C. It was directly used for further reactions.

Synthesis of the SiO_2·APS^+·Au·$Citrate^-$ Composite. A total of 210 mg (wet weight) of the SiO_2·APS^+Cl^- particles (APS = 3-Ammoniumpropylsilyl) from ethanol were washed with 20 mL of water and then dispersed in 20 mL of water. The pH of the dispersion was adjusted to 5.0 by titration with 0.01 M HCl. A total of 1.0 mL of this dispersion was added dropwise with stirring to 20 mL of the raw gold nanoparticle solution, whose pH was also about 5. During the addition, the mixture becomes hazy and the color does change to dark red. After 5 min, the solution was centrifuged at 3000 rpm and the deep-red solid was first washed with 20 mL of water and then with 2 × 20 mL of methanol. The solid was dispersed in 20 mL of methanol to yield a pink-red solution, which was used for further experiments. Elemental analysis of the dried solid (energy dispersive spectrometry, EDS): Si, 38.3 ± 1.1%; O, 44.8 ± 3.1%; Au, 16.9 ± 3.1%.

Reaction with Thiols. In a typical procedure, 20−25 mg of the thiol was added to 1.0 mL of the stirred dispersion of the composite in methanol. This produced an immediate color change to purple/blue, depending on the chain length of the alkane group. If submicromolar quantities of the thiols were used, the color change was visible only after about 5−10 min. The reaction was completed by heating to 80 °C for 5 min, and the thiol-ligated composites were then isolated by *mild* centrifugation (2000 rpm) and washed with 3 × 20 mL of methanol to remove excess thiol. For storage and for further reactions with additional thiols, the particles were dispersed in 1.0 mL of methanol. UV−vis spectra were recorded from dispersions of the particles in methanol. Elemental analysis for the dried solid from the reaction with hexanethiol (EDS): Si, 36.2 ± 1.6%; O, 48.6 ± 1.5%; Au, 15.2 ± 2.5%.

Optical and Electron Microscopy Measurements. Optical and electron microscopy measurements were performed in quartz ampules using a Hewlett-Packard 8450A UV−vis spectrometer. Samples for electron microscopy (scanning electron microscope, SEM, FEI XL30-SFEG) were prepared by drop-coating the dispersion of the respective nanoparticle composites onto 25-mm^2 pieces of a silicon wafer or on aluminum stubs. Elemental analyses were performed with an EDAX element dispersive X-ray spectroscopy system that was connected to the SEM.

Raman Spectra. Raman spectra were collected using a frequency-doubled Nd:YAG pumped (2 W, Millennia Vs, Spectra Physics), Ti:sapphire laser operating in the CW mode. The central wavelength was set to 780 nm, and the bandwidth was ∼1.0 nm. Details of this oscillator have been described elsewhere.[27] The laser beam was first sent through an air-spaced Fabry−Perot etalon (VLOC) and then through two narrowband filters (Coherent Photonics, 790 BP). After these two filters, the light intensity beyond the 20-nm bandwidth was attenuated by more than 10^7. The filtered light was then sent into a homemade inverted microscope equipped with a Raman filter (Omega Optical, 793 AELP). The light was focused onto the sample by a microscope objective (Ziess Acroplan 0.8 NA 63×) after the dichroic Raman filter. The backscattered light from the sample was collected using the same objective. This light was then focused to a fiber, which coupled the light into a spectrometer (Acton, SpectraPro 300i), and was detected by a charge-coupled device (Roper Scientific, PI-LCX 576). Spectra resolution is estimated at 15−20 cm^{-1}. The power at the sample was 10−15 mW, and the focal spot size was smaller than 3 μm. The power density at the sample was 1.4×10^5 to 2.1×10^5 W cm^{-2}. A 5000-s total acquisition time was used to acquire both Raman spectra of a pure hexanethiol and the SiO_2·Au samples. Raman spectra were collected for 100 s of each acquisition, and the spectra were subsequently summed using WinSpec32 (Roper Scientific, version 2.5.12.0) to equal a 5000-s total acquisition time.

Results and Discussion

Core−shell-type SiO_2·Au nanoparticle clusters form by reaction of 3-aminopropylsilyl-modified silica spheres with a solution of citrate-coated gold nanoparticles at pH = 5. The composites were isolated by centrifugation and stored as dispersions in methanol. According to scanning electron micrographs (Figure 2A), composite particles consist of

(23) Israelachvili, J. N. *Intermolecular and surface forces*, 2nd ed.; Academic Press: London, 1992; p 176.

(24) Omar, M. A. *Elementary solid-state physics: principles and applications*; Addison-Wesley Publishing Co.: Reading, MA, 1975; Chapter XV, p 669.

(25) Stoeber, W.; Fink, A.; Bohn, E. *J. Colloid Interface Sci.* **1968**, *26*, 62−69.

(26) Frens, G. *Nature* **1973**, *241*, 20.

(27) Cheng, G. J.; Shan, F.; Freyer, A.; Guo, T. *Appl. Opt.* **2002**, *41*, 5148−5154.

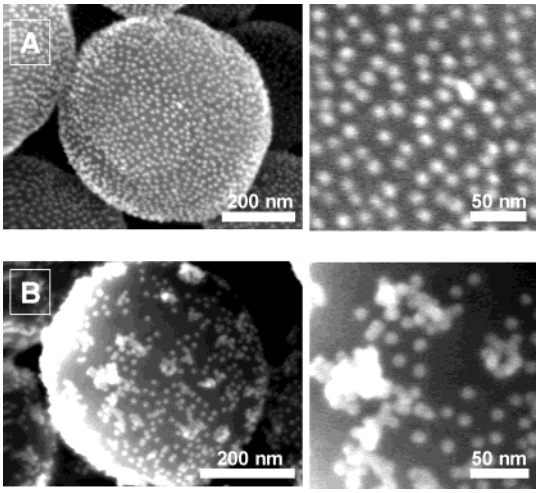

Figure 2. Morphology of the gold−silica core−shell-type composite as observed by the SEM: (a) as-synthesized, and (b) after 10 min of treatment with an aqueous solution of 0.01 M of potassium bromide.

470 ± 40 nm silica cores, whose surfaces are coated with 9.7 ± 1.0 nm citrate-ligated gold nanoparticles. Each gold particle occupies a surface area of 380 nm^2 on the silica sphere, which corresponds to 1800 gold nanoparticles per silica sphere. The separations between the gold nanoparticles are enforced by Coulomb repulsion effects between negatively charged gold particles. Similar repulsion effects have been observed in gold nanoparticle arrays on highly oriented pyrolytic graphite and silicon surfaces by Johnson et al.[28] and independently by Natan et al.[29] Additional support for an electrostatic binding model is provided by the outcome of the reaction of the core−shell-type aggregates with electrolytes such as dilute (0.1 M) hydrochloric acid or potassium bromide. Addition of these agents causes detachment of the gold nanoparticles (see Figure 2B) from the silica surface within minutes and leads to the formation of gold nanoparticle aggregates.

The gold detachment occurs because electrolytes attenuate the electrostatic fields of the respective nanoparticles,[30] and, as a consequence, the attractive silica−gold and repulsive gold−gold interaction energies are reduced. The random shapes of the formed gold nanoparticle aggregates suggest that the Au nanoparticle clustering occurs via collision of discrete SiO_2·Au composite particles rather than by diffusion of the gold nanoparticles on the surface of the silica.

A diffusion-driven structural reorganization of the silica−gold core−shell composite particles can be observed when alkanethiols $C_nH_{2n+1}SH$ ($n = 2, 3, 4, 5, 6, 8, 10, 12, 18$) are reacted with dispersions of the composite in methanol over the course of 5 min at 80 °C. Under the influence of the alkanethiols, the gold nanoparticles begin to migrate on the surface of the silica sphere. In the case of short-chain thiols C1−C4 (Figure 3A), this leads to mostly stringlike gold nanoparticle arrangements and a few two-dimensional gold nanoparticle islands, whereas thiols with longer alkylchains (C5−C18) preferentially produce two-dimensional islands of Au nanoparticles (Figure 3B−D). This hexagonal packing in these islands

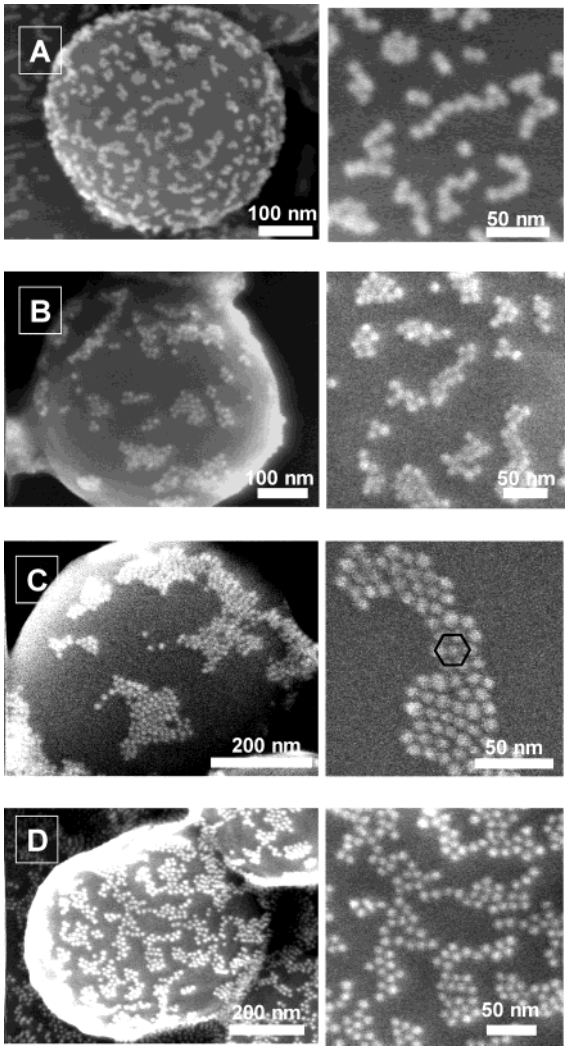

Figure 3. Scanning electron micrographs of SiO_2·Au nanoparticle clusters after reaction with alkanethiols of variable alkane group lengths: (A) propanethiol, (B) hexanethiol, (C) dodecanethiol, and (D) octadecanethiol. Magnified regions of the corresponding clusters are shown on the right.

is characteristic for weakly interacting surfactant-coated nanoparticles. This and a qualitative trend of increasing separations between gold nanoparticles with increasing length of the alkyl group suggest that the gold nanoparticles in the islands are coated by self-assembled monolayers (SAMs) of hydrophobic thiols. The position of the gold plasmon band in the clusters affords good measure of the gold nanoparticle packing distance in the two-dimensional islands. From the absorption spectra shown in Figure 4, it can be seen that the absorption maxima of the SiO_2·Au clusters undergo a bathochromic shift and line broadening upon reaction with the thiols. A plot of the absorption maxima against the length of the thiols in their stretched conformation reveals an inverse dependence of the gold plasmon resonance on the length of the thiol (Figure 5). Short-chain thiols cause a large red shift of the absorption maximum whereas long-chain thiols cause a small shift.

A qualitative understanding of this optical effect can be attained using free electron theory for metal particles. As previously discussed by Heath et al. for a two-dimensional array of silver nanoparticles,[31] the metal nanoparticle

(28) Sato, T.; Brown, D.; Johnson, B. F. G. *Chem. Commun.* **1997**, 1007−1008.

(29) Grabar, K. C.; Smith, P. C.; Musick, M. D.; Davis, J. A.; Walter, D. G.; Jackson, M. A.; Guthrie, A. P.; Natan, M. J. *J. Am. Chem. Soc.* **1996**, *118*, 1148−1153.

(30) Meyers, D. *Surfaces, Interfaces, and Colloids: Principles and Applications*; VCH Publishers: New York, NY, 1991; Chapter XIV, p 433.

(31) Heath, J. R.; Knobler, C. M.; Leff, D. V. *J. Phys. Chem. B* **1997**, *101*, 189−197.

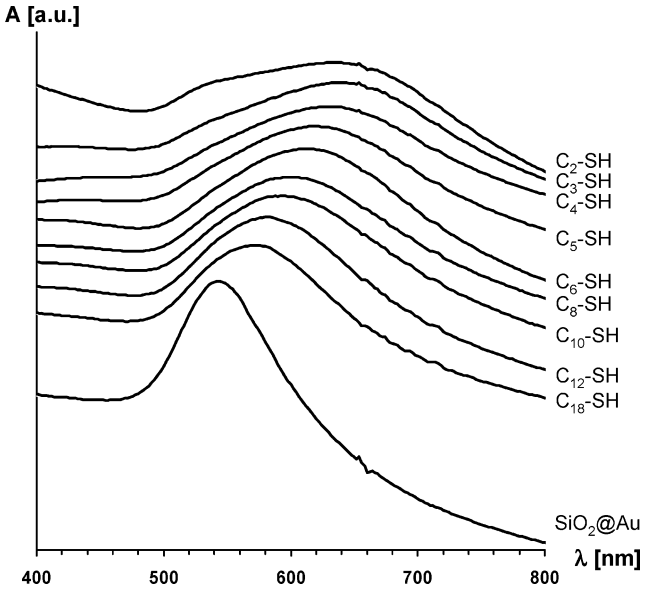

Figure 4. Electronic spectra of SiO_2·Au clusters before (bottom) and after reaction with alkanethiols $C_nH_{2n+1}SH$ (n = 2, 3, 4, 5, 6, 8, 10, 12, 18). All spectra were corrected for turbidity by subtracting the spectrum of pure SiO_2 particles in methanol.

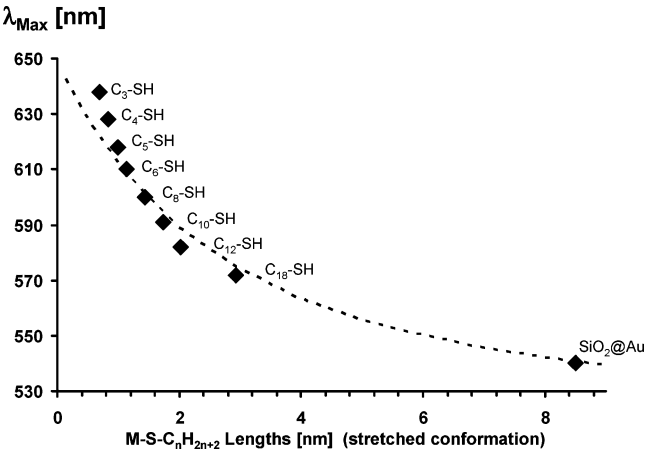

Figure 5. Experimentally observed positions of the UV−vis absorbance maxima plotted versus the lengths of the thiols (diamonds) and theoretical fit (see main text, broken line).

plasmon frequency is a function of the dielectric constant ϵ_r of the surrounding medium according to $\omega_p = [Ne^2/(m_e\epsilon_r\epsilon_0)]^{1/2}$.

Here, N is the number density of conduction electrons for gold, e is the electron charge, m_e is the electron mass, and ϵ_0 is the vacuum permittivity. As the dielectric constant of the surrounding medium increases (as would be expected for a metal particle surrounded by other metal particles instead of hydrocarbons), the plasmon band shifts to lower energy leading to a bathochromic shift of the absorption wavelengths. In a first approximation, the value of ϵ_r will be a linear function of the distance between adjacent gold nanoarticles, which will be determined by the length L of the thiol spacer in its stretched conformation. Using the inverse relationship $\epsilon_r \sim L^{-1}$, it is possible to fit the data with the theoretical curve shown in Figure 5 (for details of the calculation see Supporting Information). Refined models for three-dimensional and two-dimensional metal nanoparticle arrays, using effective medium theory for the calculation of the dielectric functions of gold particle aggregates, have been formulated by Storhoff et al.,[32] Collier et al.,[33] and Lazarides and Schatz.[34]

Element-dispersive X-ray spectra (Supporting Information) of the SiO_2·Au composites before and after reaction with hexanethiol show that the Au/Si/O compositions are not affected by reaction with the thiol. The mean gold content of 16.1% in these samples translates into 2500 ± 170 gold particles per silica sphere, which is in satisfactory agreement with morphology of the composite particles as determined by the SEM (see previous). Carbon could not be detected in the samples. Because of the low thiol concentration, it is difficult to obtain direct spectroscopic evidence for the presence of the thiols in the composite. IR spectra of the thiol-treated SiO_2·Au composites (Supporting Information), for example, are dominated by a strong Si−O stretching vibration from the SiO_2 particles but show no contributions from coordinated thiols. Raman spectroscopy, on the other hand, has a much higher sensitivity because of the surface-enhanced Raman scattering (SERS) effect due to the gold nanoparticles. Figure 6 shows Raman spectra for the SiO_2·Au after reaction with hexanethiol and for free hexanethiol.

The spectra of the thiol-reacted SiO_2·Au composite and of the pure thiol contain several characteristic peaks. The fact that the weak H−S peak at 2550 cm^{-1} is absent in the SiO_2·Au composite can be taken as an indication that the thiol is bonded to the gold nanoparticles via the Au−S bond and not just intercalated into the colloidal aggregate. The formation of a thiol-SAM is also supported by the disappearance of the C−S gauche at ∼650 cm^{-1} after binding to the Au nanoparticles[38,39] and by the disappearance of the methylene C−H stretching modes (the broad peak between 2800 and 2900 cm^{-1}), whereas the methyl C−H stretching mode (the peak at 2950 cm^{-1}) is affected only slightly.

A simple estimation (Supporting Information) shows that the concentration of thiol molecules in the SiO_2·Au composite is reduced by 2−3 orders of magnitude when compared to that of a sample of the pure thiol. Taking the probing volume into consideration, the total enhancement factor is larger than 10^5. This supports that the Raman signal from the SiO_2·Au sample is surface-enhanced by individual gold nanoparticles.[35−37]

Mechanistically, the conversion of the ordered structure shown in Figure 2A into the disordered structures shown in Figures 3 involves at least two steps, the formation of a thiol SAM on the gold surface and the subsequent diffusion of nanoparticles on the silica surface. In this regard, it is informative to compare the interaction energies of gold and silica nanoparticles before and after the reaction with alkanethiols. Previous calculations estimate the electrostatic interaction energy between a negatively charged citrate-ligated gold nanoparticle and a positively charged, alkylammonium-derivatized silica particle to be on the order of -10^{-18} J per particle dimer (-10^3 kJ/mol of particle dimers).[8,40] The accuracy of this

(32) Storhoff, J. J.; Lazarides, A. A.; Mucic, R. C.; Mirkin, C. A.; Letsinger, R. L.; Schatz, G. C. *J. Am. Chem. Soc.* **2000**, *122*, 4640−4650.
(33) Collier, C. P.; Vossmeyer, T.; Heath, J. R. *Annu. Rev. Phys. Chem.* **1998**, *49*, 371−404.
(34) Lazarides, A. A.; Schatz, G. C. *J. Phys. Chem. B* **2000**, *104*, 460−467.
(35) Siiman, O.; Bumm, L. A.; Callaghan, R.; Blatchforg, C. G.; Kerker, M. *J. Phys. Chem.* **1983**, *87*, 1014.
(36) Hu, J. W.; Zhao, B.; Xu, W. Q.; Fan, Y. G.; Li, B.; Ozaki, Y. *Langmuir* **2002**, *18*, 6839−6844.
(37) Moskovits, M. *Rev. Mod. Phys.* **1985**, *57*, 783.
(38) Bryant, M. A.; Pemberton, J. E. *J. Am. Chem. Soc.* **1991**, *113*, 8284−8293.
(39) Compagnini, G.; Galati, C.; Pignataro, S. *Phys. Chem. Chem. Phys.* **1999**, *1*, 2351−2353.
(40) Evans, D. F.; Wennerström, H. *The Colloidal Domain: Where Physics, Chemistry, Biology, and Technology Meet*, 2nd ed.; Wiley-VCH: New York, 1999; p 413.

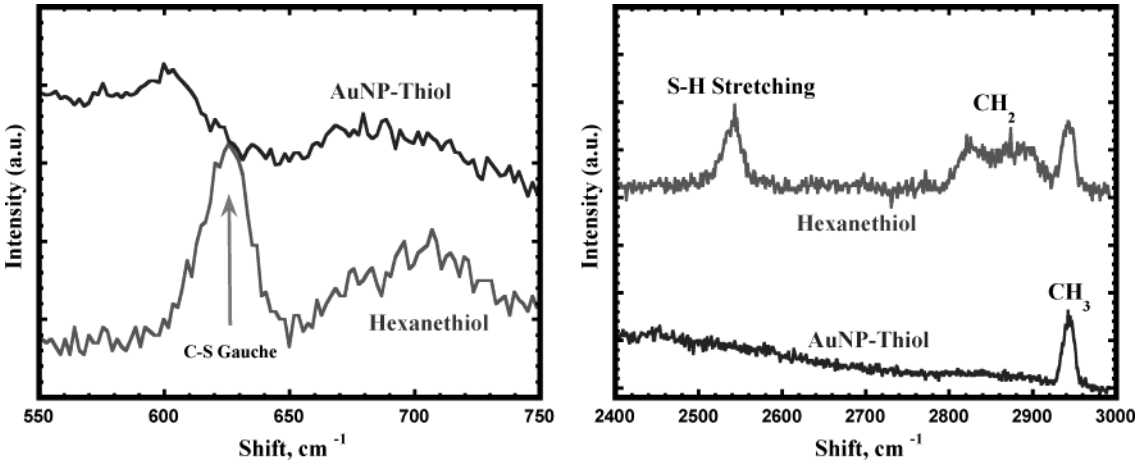

Figure 6. Comparison of SERS spectra for the SiO_2·Au−SC_6H_{13} composite and for pure hexanethiol. The weakness of the C−H bands in the spectra is due to the reduced detection sensitivity of the analytical setup at 1.00 mm, which is five times weaker than at 800 nm.

value is limited because the concentration of negative groups (citrate, chloride, hydroxide) on the gold nanoparticle surface is not known exactly. As the charge of the gold particles is annihilated by reaction with alkanethiols,[12] the coulomb attraction term becomes zero and the interaction between gold and silica becomes primarily of the van der Waals type, although a residual charge-dipolar interaction between the neutral gold particle and the positively charged alkylammonium groups on the silica surface cannot be ruled out. The van der Waals interaction energy between two spheres is described by $W = -(A/6D)[R_1R_2/(R_1 + R_2)]$ with $R_{1,2} = 4.85$, 235 nm for the radii of the interacting spheres and $D = 1$ nm as the distance between the interacting particles.[23] Because the van der Waals interactions between gold and silica in methanol will be dominated by the surface-immobilized aliphatic groups, it is reasonable to use the Hamaker constant $A = 0.5 \times 10^{-20}$ J for interactions between hydrocarbons in a polar medium.[23] One obtains $W = -4.0 \times 10^{-21}$ J (−2.4 kJ/mol) for the interaction energy of the gold−silica particle dimer. This value is ∼400 times smaller than the electrostatic interaction energy, and it is similar to the average thermal energy of a molecule kT (5×10^{-21} J or 3 kJ/mol at 80 °C). This agrees with the possibility of thermally activated diffusion of gold nanoparticles on the silica surface. The removal of gold particles from the silica surfaces does not occur, because the thiol-ligated gold particles have very little solubility in the hydrophilic solvent methanol.

The structural and optical changes observed in SiO_2·Au clusters upon reaction with thiols are (a) characteristic of the alkanethiol, (b) fast at 80 °C, and (c) occur at micromolar concentrations of the thiols. In the reaction of 0.3 mg of SiO_2·Au with $C_6H_{13}SH$, for example, a color change is noticeable with as little as 2−5 nmol of the thiol, although the reaction needs minutes to complete because of the slower kinetics of the SAM formation. These characteristics establish SiO_2·Au clusters as a primitive coulometric sensor for the qualitative detection of alkanethiols. An important difference to other known nanomaterial-based sensors is that the optical changes of the material are not a direct result of binding of the analyte but that they are caused instead by a *structural reorganization* of the material. This distinguishes the present system from other nanomaterial-based sensors (nanowires,[41−44] porous silicon,[45,46] magnetite nanoparticles,[47] carbon nanotubes,[48] gold nanoparticle films)[49] in which binding of the analyte causes a *direct* change of a physical property of the sensing material, for example, its conductivity, color, magnetism, or resonance frequency.

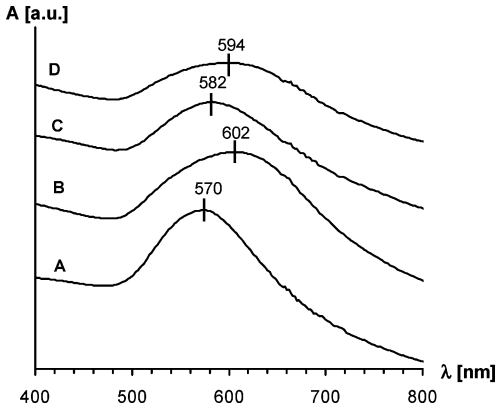

Figure 7. UV−vis spectra of a single sample of SiO_2·Au clusters after successive reaction with octadecanethiol (A, C) and butanethiol (B, D). All spectra were corrected for turbidity by subtracting the spectrum of pure SiO_2 particles in methanol.

A drawback of the SiO_2·Au system is its irreversibility. An alternating treatment of the silica−gold composite with two different alkanethiols preserves the structural integrity of the van der Waals assembled SiO_2·Au clusters, but the corresponding changes in the optical spectra become less characteristic of the thiol. This is shown in Figure 7 for alternating reactions of the SiO_2·Au aggregate with octadecanethiol and butanethiol. The addition of C_4H_9SH to $C_{18}H_{37}SH$-pretreated SiO_2·Au clusters still produces a small but noticeable shift of the absorption

(41) Kong, J.; Franklin, N. R.; Zhou, C. W.; Chapline, M. G.; Peng, S.; Cho, K. J.; Dai, H. J. *Science* **2000**, *287*, 622−625.
(42) Kong, J.; Chapline, M. G.; Dai, H. J. *Adv. Mater.* **2001**, *13*, 1384−1386.
(43) Cui, Y.; Wei, Q. Q.; Park, H. K.; Lieber, C. M. *Science* **2001**, *293*, 1289−1292.
(44) Favier, F.; Walter, E. C.; Zach, M. P.; Benter, T.; Penner, R. M. *Science* **2001**, *293*, 2227−2231.
(45) Janshoff, A.; Dancil, K. P. S.; Steinem, C.; Greiner, D. P.; Lin, V. S. Y.; Gurtner, C.; Motesharei, K.; Sailor, M. J.; Ghadiri, M. R. *J. Am. Chem. Soc.* **1998**, *120*, 12108−12116.
(46) Song, J. H.; Sailor, M. J. *J. Am. Chem. Soc.* **1997**, *119*, 7381−7385.
(47) Chemla, Y. R.; Crossman, H. L.; Poon, Y.; McDermott, R.; Stevens, R.; Alper, M. D.; Clarke, J. *Proc. Natl. Acad. Sci. U.S.A.* **2000**, *97*, 14268−14272.
(48) Chopra, S.; Pham, A.; Gaillard, J.; Parker, A.; Rao, A. M. *Appl. Phys. Lett.* **2002**, *80*, 4632−4634.
(49) Wuelfing, W. P.; Murray, R. W. *J. Phys. Chem. B* **2002**, *106*, 3139−3145.

maximum to 602 nm (instead of 630 nm), but the subsequent addition of octadecanethiol fails to shift the absorption maximum of the thiol-ligated SiO_2·Au cluster back to the original value.

A possible explanation of this behavior is based on the size difference between the thiols and on the packing density of the Au clusters in the two-dimensional islands. While the shorter *n*-butanethiol manages to displace at least some of the $C_{18}H_{37}SH$ from the gold surfaces, the reverse is not possible because of the spatial constraints of the two-dimensional cluster aggregate: There is not enough room between gold particles in the two-dimensional island to accommodate a larger alkanethiol.

In conclusion, we have shown that the reaction of nanoparticle composites with molecules and ions can lead to characteristic changes of the bonding between nanoparticles, of the structure of the nanoparticle aggregate, and of its optical properties. Chemically induced processes, like the one described, are relevant to the design of nanoscale chemical switches and sensors and to the construction of nanoparticle-based machines.

Acknowledgment. This work was supported by a type G starter grant of the Petroleum Research Fund (38057-G5) and by startup funds of the University of California, Davis.

Supporting Information Available: IR spectra, optical micrographs, EDS spectra, and theoretical fit of the UV−vis absorption spectra. This material is available free of charge via the Internet at http://pubs.acs.org.

LA0348719